STOCHASTIC DOWNSCALING EXPERIMENTS FOR SOUTHWEST WESTERN AUSTRALIA

Bryson C. Bates[1], Stephen P. Charles[1] and Edward P. Campbell[2]

[1]CSIRO Land and Water

[2]CSIRO Mathematical and Information Sciences

Second Research Phase Report

for the

Indian Ocean Climate Initiative

TABLE OF CONTENTS

LIST OF TABLES

LIST OF FIGURES

SUMMARY

During the first three years of the Indian Ocean Climate Initiative (IOCI), CSIRO Land and Water (CLW) has:

- Examined the utility of stochastic downscaling models and prospects for their use in a statistical-physical, interseasonal climate forecasting system for southwest Western Australia (SWA).

- Used stochastic downscaling as a means of unravelling the causes of the recent low precipitation sequence over much of the region.

Downscaling may be defined as the quantification of the relation of small-scale climate variables to larger scale atmospheric patterns. These patterns may be observed or simulated by general circulation models (GCMs).

Our studies for IOCI Second Research Phase (July 1999 – December 2000) have again focused on the application of an extended nonhomogeneous hidden Markov model (NHMM) to daily May to October precipitation across a network of 30 stations scattered throughout SWA. This model was selected on the basis of its documented performance and generality.

The original set of goals proposed by CLW for IOCI Second Research Phase were (IOCI, 1999):

- The development of a new NHMM framework that considers precipitation amounts and occurrences jointly.

- Investigation of the stationarity of NHMM parameters using global mean sea level pressure (MSLP) data sets.

- Driving the NHMM with global MSLP data sets to obtain insight into the long-term, temporal and spatial changes in historical synoptic patterns over SWA.

- Investigation of the relationship between the changes in synoptic patterns over time and the observed secular breaks in SWA precipitation.

- A new study of potential predictability using the new NHMM, the Mark 3 version of the CSIRO GCM and an updated historical sea surface temperature (SST) data set.

- For GCM grid cells around SWA, investigation of the interdecadal variability in a 1000-year, CSIRO9 Mark 2 GCM run with a view to detecting any secular changes in modelled atmospheric series and downscaled precipitation series and identifying their causes.

Five factors led to modification of the above goals. These factors were:

- The development and testing of the new NHMM framework described above by our collaborators at the National Center for Statistics and the Environment, University of Washington, Seattle. The new framework did not provide a noticeable improvement in model performance. Consequently, we continued our research efforts with the original model.

- The advent of the National Center for Atmospheric Research (NCAR) – National Centers for Climate Prediction (NCEP) Reanalysis dataset containing global atmospheric fields for the period 1958-1998. This dataset encompasses the timing of the low inflow sequence for the Perth water supply system and the period used for estimating the parameters of the NHMM (1978-1992). The Reanalysis dataset was derived by assimilating observed atmospheric data with a high resolution GCM.

- The postponement of the CSIRO Mark 3 GCM runs described above.

- An evaluation of the NHMM using the Reanalysis dataset that led to a revision of the set of atmospheric variables used by the model.

- A promising line of investigation regarding the cause of the low precipitation sequence over SWA.

Consequently the research goals pursued by CLW during IOCI Second Research Phase were:

- Evaluation of the NHMM using the Reanalysis dataset. This work would reveal any deficiencies in the NHMM and provide insight into the stationarity of its parameters.

- Following successful evaluation of the NHMM, investigation of the long-term temporal changes in historical synoptic patterns over SWA and thus identification of the cause of the observed secular breaks in SWA precipitation.

- Downscaling the 1000-year, CSIRO Mark 2 GCM run with a view to characterising the probability of the observed low precipitation sequence.

Our achievements and preliminary conclusions include:

- After revision of the set of atmospheric predictor variables used in the NHMM, it was found that NHMM parameter estimates derived from atmospheric and precipitation data for the period 1978 to 1992, inclusive, could be used to simulate monthly precipitation over SWA for the period 1958-1998. This suggests that the NHMM is robust against secular breaks in atmospheric circulation and precipitation, and that it may be a useful tool for downscaling an interseasonal climate forecast produced by a GCM.

- Analysis of the results obtained from the NHMM revealed an abrupt shift and a clearly defined trend in the frequency characteristics of synoptic patterns that influence precipitation occurrence over SWA. The timing and nature of these changes are consistent with the characteristics of the observed low precipitation sequence.

- The timing of the shift appears to coincide with the well-documented change in the behaviour of the El Niño – Southern Oscillation that occurred in the mid 1970s. The trend appears to be due to a different mechanism, and may be related to changes in the behaviour of the Antarctic Oscillation and an interaction between the Oscillation and El Niño.

- The changes in the frequency characteristics of the synoptic patterns and the resultant low precipitation sequence since the mid 1970s are due to changes in a combination of atmospheric variables reflecting the location and intensity of low and high pressure

systems, and the moisture content of the lower troposphere. The low precipitation sequence cannot be ascribed to change(s) in a single variable such as MSLP.

- Results from the downscaled 1000-year GCM run suggest the recent low precipitation sequence over SWA is uncommon but not extreme.

Future work will involve:

- Downscaling interseasonal climate forecasts from the coupled ocean-atmosphere CSIRO Mark 3 GCM for the winters of 2000 and 2001. This work will provide information about the reliability of forecasts and forecast lead-times.

- Exploring the Reanalysis dataset with a view to identifying the large-scale climatic forcing responsible for the low precipitation sequence since the mid 1970s. This work will involve a detailed investigation of the effects of El Niño and the Antarctic Oscillation on SWA precipitation.

Outcomes from this work will include:

- An assessment of the utility of downscaled, interseasonal climate forecasts from coupled ocean-atmosphere GCMs.

- Further insight into the large-scale climatic forcing that has caused the low precipitation sequence.

ACKNOWLEDGEMENTS

1. INTRODUCTION

1.1 Downscaling Climate Model Simulations

Modelling the response of natural and agricultural systems to climate forecasts requires daily data at local and regional scales. The need for improved quantitative precipitation forecasts, and realistic assessments of the regional impacts of natural climate variability and possible climate change due to the enhanced greenhouse effect, has generated increased interest in regional climate simulation. Although existing general circulation models (GCMs) perform reasonably well in simulating climate with respect to annual or seasonal averages at sub-continental scales, it is widely acknowledged that they do not provide credible simulations of precipitation at the space and time scales relevant to local and regional impact analyses (Arnell *et al.*, 1996; Gates *et al.*, 1996).

The above problems have led to the development of statistical downscaling techniques to derive sub-grid scale weather from the coarse spatial resolution atmospheric data available from GCMs. Downscaling techniques include:

- Modelling the daily precipitation process through multivariate probability distributions conditional on explicitly derived, large-scale atmospheric circulation patterns (e.g., Bardossy and Plate, 1991, 1992; Bogardi *et al.*, 1993).

- Regressions on continuous atmospheric circulation indices, geographic location and topographical variables (Enke and Spekat, 1997; Huth, 1997; Wilby *et al.*, 1998).

- Artificial neural networks (e.g., Crane and Hewitson, 1998).

- Hidden Markov models (see below)

1.2 Nonhomogeneous Hidden Markov Model (NHMM)

The downscaling method used herein consists of a nonhomogeneous hidden Markov model (NHMM) to simulate precipitation occurrence and multiple linear regression to simulate precipitation amounts in southwest Western Australia (SWA) (Hughes *et al.*, 1999; Charles *et al.*, 1999). Recall from IOCI (1999) that the NHMM relates synoptic-scale, atmospheric

circulation variables through a finite number of hidden (unobserved) weather states to multi-site, daily precipitation occurrence data. The NHMM determines the most distinct patterns in a daily multi-site precipitation occurrence record rather than patterns in atmospheric circulation. These patterns are then defined as conditionally dependent on a set of atmospheric predictor variables. The weather states are not defined *a priori*. A first-order Markov process defines the daily transitions from weather state to weather state. The process is described as nonhomogeneous as the transition probabilities are conditional on a set of atmospheric circulation predictors. The atmospheric predictors may include raw variables such as mean sea level pressure (MSLP) or derived variables such as north-south MSLP gradient. In this way, the NHMM captures much of the spatial and temporal variability of the precipitation occurrence process.

Model selection involves sequential fitting of several NHMMs with an increasing number of weather states and atmospheric predictors. The fit is evaluated in terms of the physical realism and distinctness of the identified weather states as well as a Bayesian information criterion (BIC). The objective is to select a NHMM that minimises the BIC, thus identifying a relatively parsimonious model that fits the data well. The most likely weather state sequence is obtained from the selected NHMM using the Viterbi algorithm. This permits the assignment of each day to its respective state (Hughes *et al.*, 1999). The ability to classify days into weather states that are distinct in terms of spatial precipitation occurrence pattern as well as synoptic situation means that the physical realism of the states can be assessed.

The joint distribution of daily precipitation amounts at multiple sites is evaluated through the specification of conditional distributions for each site and weather state (Charles *et al.*, 1999). The conditional distributions consist of regressions of transformed amounts at a given site on precipitation occurrence at neighbouring sites within a set radius. An automatic variable selection procedure is used to identify the neighbouring sites that provide useful information about at-site precipitation amounts. The neighbourhood radius is determined by steadily increasing its size until further increases result in marginal improvements in the proportion of total precipitation variability explained by the precipitation occurrences at neighbouring sites.

1.3   General Circulation Model

In this report we used a 1000-year run from the Mark 2 version of the spectral 9-level atmospheric GCM developed by the CSIRO Atmospheric Research (hereafter referred to as CSIRO9 GCM) at a horizontal resolution of R21 (roughly 700 km). Descriptions of the model can be found in McGregor *et al*. (1993) and IOCI (1999).

2. DESCRIPTION OF STUDY AREA AND DATA

We defined SWA as the region extending from about 30° to 35° south and 115° to 120° east (Figure 2.1). For the stations depicted in Figure 2.1, the percentage of annual precipitation that falls in the period from May to October varies from 66 to 86%: 25 stations have percentages greater than 71%. The majority of winter rains come from low pressure frontal systems. Thus we divided the year into the winter half-year (May-October) and summer half-year (November-April) seasons. A full set of results for the winter half-year is presented in this report.
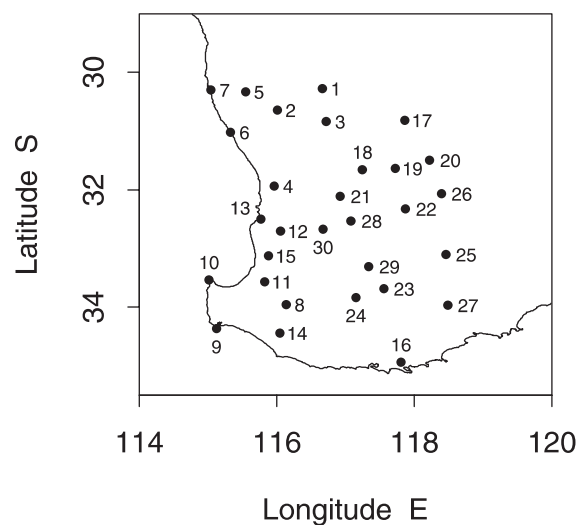
Figure 2.1   **Location of daily precipitation stations in southwest Western Australia (for key to numerals see Table 2.1).**

In our earlier work, the NHMM was fit to atmospheric and daily precipitation data for the period from 1978 to 1992. The data were obtained from the Bureau of Meteorology. Twenty-five atmospheric variables were derived from this data set, and the data interpolated to a rectangular 3.75° longitudinal by 2.25° latitudinal grid. An additional variable (850 hPa to 500 hPa thickness) was added to the list of candidate atmospheric predictors in 2000. The locations of the 30 precipitation stations considered are shown in Figure 2.1. A key to the numerals shown in Figure 2.1 is given in Table 2.1. These stations have no missing records over 1978-92. Further details are given in IOCI (1999).

Table 2.1   Details of Daily Precipitation Stations [Reproduced from IOCI (1999)].

No. (Fig. 2.1)	Station Name	Station No.	Elevation (m)	Annual Precipitation (mm)
1	Dalwallinu P.O.	008039	335.0	357
2	Moora (Moora Shire)	008091	203.0	461
3	Wongan Hills Res. Stn	008138	305.0	349
4	Perth Airport M.O.	009021	20.0	802
5	Dandaragan (Badgingarra Res. Stn)	009037	260.0	598
6	Lancelin	009114	4.0	627
7	Jurien	009131	2.0	560
8	Bridgetown P.O.	009510	150.0	843
9	Augusta (Cape Leeuwin A.W.S.)	009518	14.0	1000
10	Busselton (Cape Naturaliste L.H.)	009519	97.0	830
11	Donnybrook P.O.	009534	63.0	1002
12	Dwellingup (Forestry)	009538	267.0	1279
13	Mandurah (Park)	009572	15.0	888
14	Pemberton (Forestry)	009592	174.0	1213
15	Harvey (Wokalup Agric. Res. Stn)	009642	116.0	996
16	Albany A.M.O.	009741	68.0	805
17	Bencubbin (Bencubbin)	010007	353.0	320
18	Cunderdin P.O.	010035	236.0	368
19	Kellerberrin (composite)	010073	247.0	333
20	Merredin (Res. Stn)	010093	318.0	309
21	Beverley P.O.	010515	199.0	422
22	Corrigin P.O.	010536	295.0	378
23	Katanning P.O.	010579	310.0	485
24	Kojonup (composite)	010582	305.0	542
25	Lake Grace P.O.	010592	286.0	353
26	Narembeen P.O.	010612	276.0	332
27	Ongerup (Ongerup)	010622	286.0	383
28	Pingelly P.O.	010626	297.0	455
29	Wagin P.O.	010647	256.0	440
30	Wandering (Shire)	010648	280.0	626

Most of our analyses for IOCI Second Research Phase were based on the National Center for Atmospheric Research (NCAR) – National Centers for Climate Prediction (NCEP) Reanalysis dataset (Kalnay *et al*., 1996). The dataset contains a long record of global

analyses of atmospheric fields for the 41-year period from 1958 to 1998. Data are available at 0000, 0600, 1200, and 1800 GMT on a 2.5° latitude-longitude grid. The Reanalysis project involved the recovery of land surface, rawisonde, pibal, aircraft, satellite, and other data from different countries and organisations, data quality control, and the assimilation of the data with a frozen state-of-the-art analysis/forecast system. The use of a frozen system eliminates perceived climate jumps associated with changes in the data assimilation techniques. A 28-level spectral GCM with a horizontal resolution of T62 (roughly 210 km) is used in the assimilation system. Output variables are classified into four classes ("A" to "D") depending on the degree to which the variables are influenced by observations and/or the GCM. For example, MSLP is a class "A" variable since it is strongly influenced by observational data. Humidity is a class "B" variable in that the GCM has a strong influence on its value despite the existence of observational data that directly affect it. Reanalysis data for the atmospheric predictors in the NHMM were interpolated to the grid using for NHMM fitting.

Some studies have reported spurious temporal trends in Reanalysis fields (e.g., Hines and Bromwich, 1999; Marshall and Harangozo, 1999). We screened each atmospheric predictor series for changes in mean level that were large relative to the background variability in the Reanalysis data. We used the nonparametric jump-detection algorithm proposed by Qiu and Yandell (1998) to screen each of the atmospheric predictor series for spurious jumps in their means. Predictors that exhibited departures from normality were transformed prior to analysis. Given that the daily atmospheric predictor series for each winter half-year are serially correlated, we used a small window width to reduce the dependence as far as possible.

The data from the 1000-year GCM run were interpolated to the rectangular grid described above. The historical and modelled atmospheric data were centred using their respective means. This removes the effects of any bias in the modelled means on the downscaled simulations. There did not appear to be any bias in the modelled variances. Atmospheric variables derived from the modelled data were used as input to the NHMM: the NHMM was not fit to the GCM data.

3. EVALUATION AND MODIFICATION OF DOWNSCALING MODEL

3.1 Introduction

Recall from IOCI (1999) that a 6-state NHMM with three atmospheric predictors [the mean of MSLP across five grid points (hereafter referred to as mean MSLP), north-south MSLP gradient, and dew point temperature depression at 850 hPa (DT_d^{850})] could provide credible reproductions of at-site precipitation occurrence probabilities and their spatial association, and dry- and wet-spell length statistics at the seasonal (six-monthly) scale for the gauges listed in Table 2.1. DT_d^{850} is defined as the difference between the air and dew point temperatures at 850 hPa. Therefore, it is a measure of humidity in the lower troposphere. A dry spell is defined as a sequence of consecutive days during which daily precipitation remains below 0.3 mm. A wet spell is defined as a sequence of consecutive days during which daily precipitation equals or exceeds 0.3 mm. The precipitation occurrence patterns and the composite MSLP fields associated with the weather states are given in Figure 3.1.

In this section we use the NCEP-NCAR Reanalysis dataset to evaluate the NHMM. One thousand 41-year sequences of daily May to October precipitation were generated from the fitted NHMM, conditionally on the atmospheric predictors extracted from the Reanalysis dataset. For the first time the model's performance is subjected to scrutiny on a monthly rather than a seasonal time scale, and an out-of-sample-validation over a period that is wetter than but similar in length to the fitting period. Initial results indicated that the NHMM was inadequate. It was evident that the intraseasonal variation in the atmospheric circulation over SWA had not been fully captured by the model. Further investigation led to an augmented atmospheric predictor set for the NHMM. The modified NHMM is shown to resolve most of the performance deficiencies of the original model.
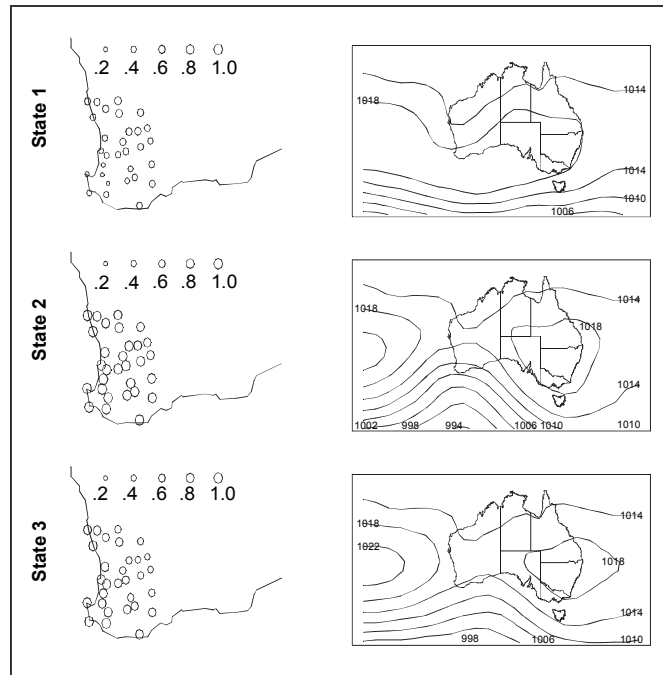
Figure 3.1(a)   Precipitation occurrence patterns and MSLP averaged over all days classified under weather states 1 to 3. The diameters of the circles indicate daily precipitation occurrence probabilities at each site.
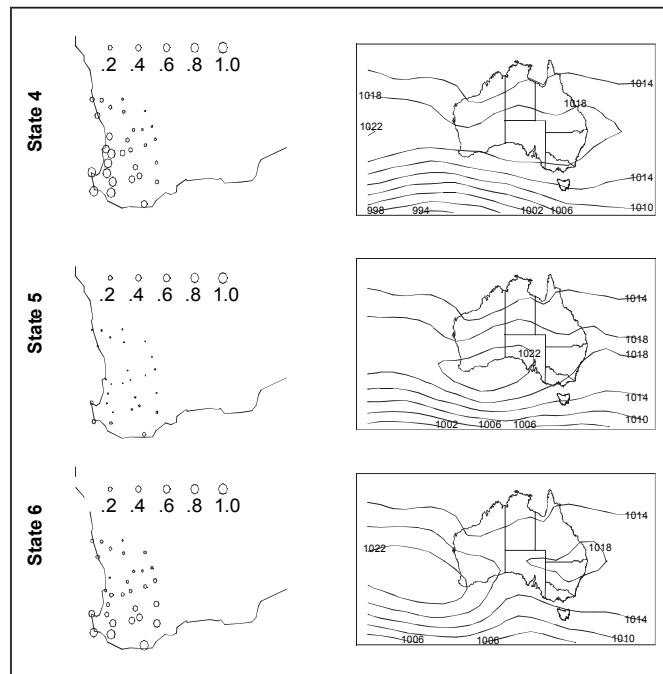
Figure 3.1(b)   Precipitation occurrence patterns and MSLP averaged over all days classified under weather states 4 to 6. The diameters of the circles indicate daily precipitation occurrence probabilities at each site.

3.2   Evaluation of the NHMM

Figure 3.2 compares the simulated daily precipitation occurrence probabilities with historical values for the 30 sites for each month in the winter half-year over the fitting period (1978-1992). The NHMM underestimates precipitation occurrence during the wettest months (June and July) and overestimates occurrence in the driest months (September and October). Performance deficiencies are also apparent for May and August. Moreover, there is a cyclical variation in the sign and magnitude of the bias in the simulated probabilities across the winter half-year.
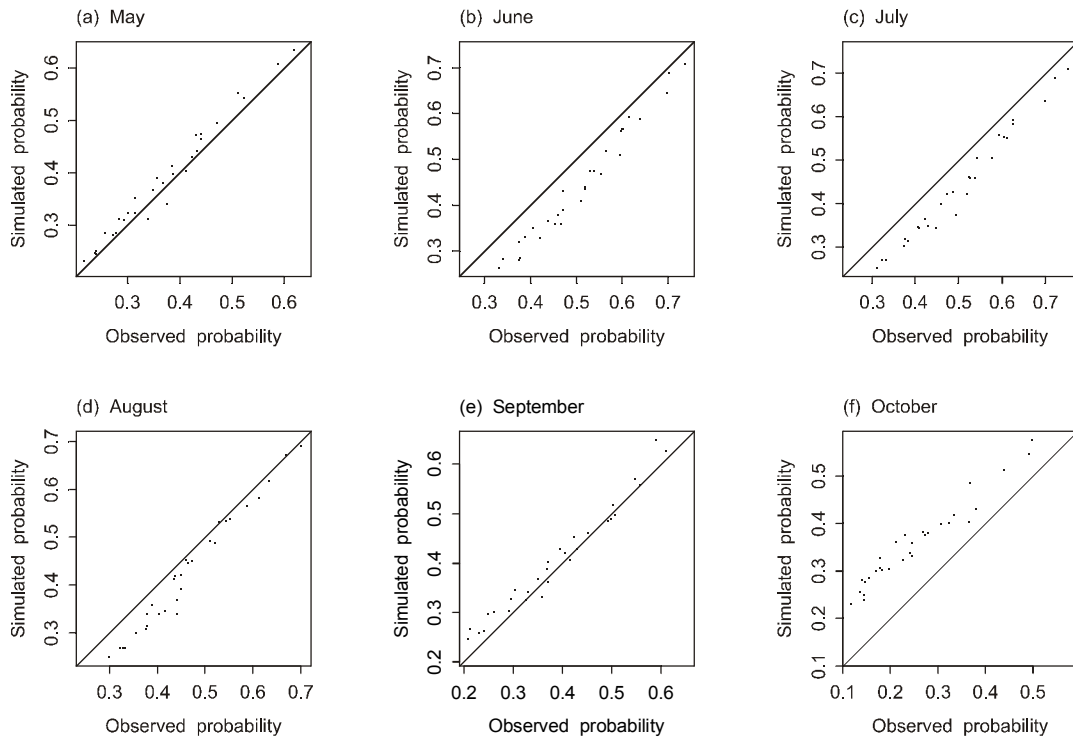
**Figure 3.2   Comparison of simulated and historical daily precipitation probabilities
for the period 1978–1992.**

Similar problems were evident in the precipitation amount simulations. The seasonal distribution of the errors in the simulation of monthly precipitation amounts for Pingelly is given in Figure 3.3. The standardised residuals (e_i) shown are defined by

$$e_i \; = \; (r_i - m_i)/s_i, \qquad i = 1, \ldots, T \qquad (1)$$

where r_i is the observed monthly precipitation amount for the ith month, m_i and s_i are the mean and standard deviation of the 1000 simulated amounts for the ith month, and

$T = 6*15 = 90$ for the 15-year fitting period. The standardised residuals exhibit a cyclical variation through the winter half-year. The simulated precipitation amounts for May and August are close to the observed, but the fit is poor to very poor for the remaining winter months. This suggests that at least one additional predictor is required for downscaling experiments at the monthly time scale.
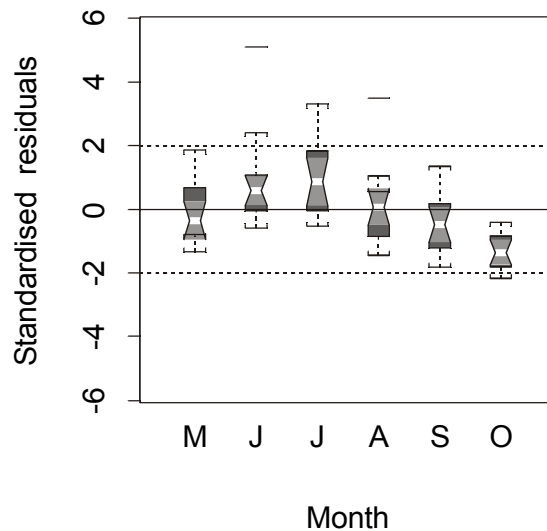
Figure 3.3   Box plots showing seasonal distribution of standardised residuals for Pingelly (Station 28) for the period 1978–1992.The edges of the boxes mark the upper and lower quartiles. The horizontal line within each box denotes the median, and the end points of the whiskers attached to each box denote the extremes. If the notches on two boxes do not overlap, this indicates a difference in location that is roughly significant at the 5% level.

An exhaustive but essentially fruitless search was undertaken to identify which of the remaining 23 atmospheric variables could account for the bias in the NHMM simulations. This suggested that the use of a combination of predictors might be required. We used canonical correlation analysis (CCA) to quantify the correlations between linear combinations of the precipitation occurrence residuals for the 30 sites and linear combinations of the atmospheric predictors for 1978-1992. In CCA, the pair of linear combinations having the highest correlation is determined first. The next pair to be considered has the highest correlation among all pairs that are uncorrelated with the first pair, and so on. The pairs of linear combinations are called canonical variables, and their correlations are called canonical correlations (Kshirsagar, 1972; Jobson, 1992).

Prior to the CCA, two atmospheric variables ("10" and "11") were removed from the predictor set since they are linear combinations of other predictors. Thus the number of canonical variables and correlations is min (30, 24) = 24. (Recall that there are 30 sites and

that there were 26 predictors before predictors "10" and "11" were dropped.) The atmospheric variables were standardised to zero mean and unit variance. The precipitation occurrence residuals are defined by

$$r_k^t = (R_k^t - p_k^t)\big/[p_k^t(1 - p_k^t)] \tag{2}$$

where $R_k^t = 1$ if precipitation is greater than or equal to 0.3 mm at gauge k on day t and 0 otherwise, and

$$p_k^t = \sum_{j=1}^{6} P(R_k^t \mid S_j^t)\, P(S_j^t) \tag{3}$$

in which the probabilities $P(R_k^t \mid S_j^t)$ and $P(S_j^t)$ are determined from the fitted NHMM. We transformed the r_k^t to normality using an inverse probit transform. The estimates of the first three estimated canonical correlations were 0.568, 0.516 and 0.326.

A bar chart of the standardised coefficients for the first atmospheric canonical variable is given in Figure 3.4. This variable has a relatively large positive coefficient for variable "1" (mean MSLP), and relatively large negative coefficient for variable "2" (mean geopotential height at 500 hPa), and moderate positive coefficients for variables "7" (east-west MSLP gradient), "25" (850 hPa to 500 hPa thickness), and "26" (DT_d^{850}).
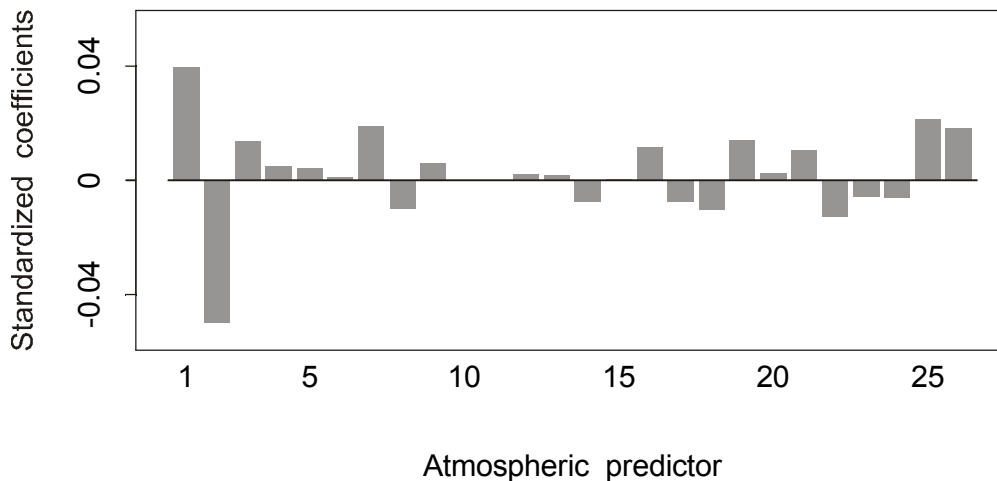
Figure 3.4   Bar chart of standardised coefficients for the first atmospheric canonical variable (for completeness, coefficients for variables "10" and "11" are shown as zero.)

A map of the standardised coefficients for the first precipitation occurrence residual canonical variable (hereafter called the first residual canonical variable) is given in Figure 3.5. Stations with large negative coefficients are concentrated along the south coast of SWA. Stations with large positive coefficients are located in the northeast corner of SWA and along the west coast. Thus the first residual canonical variable contrasts the error in the NHMM fit for stations along the south coast with that for the northeast corner and west coast. The moderate positive correlation between the first residual and atmospheric canonical variables suggests that this contrast is higher when centred mean MSLP, east-west MSLP gradient and DT_d^{850} are large relative to centred mean geopotential height at 850 and 500 hPa. Thus if rainfall occurs over SWA, it is more likely to occur in the north rather than the south due to the presence of a midlevel trough over the region or to the west. When centred mean MSLP, east-west MSLP gradient and DT_d^{850} are small relative to centred mean geopotential height at 850 and 500 hPa, rainfall will tend to occur in the south relative to the north due to a high pressure system situated to the west of SWA with a ridge forming along the south coast.
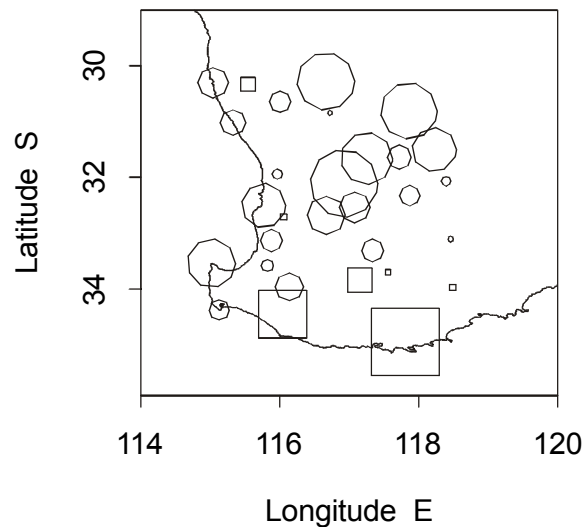
Figure 3.5 **Map of standardised coefficients for the first precipitation occurrence residual canonical variable. Circles denote positive coefficients and squares negative coefficients. The diameter of the circles and the lengths of the sides of the squares are in direct proportion to the magnitude of the coefficients.**

Figure 3.6 shows box plots of the first canonical variables for each month in the winter half-year. A seasonal cycle in both variables is apparent, and it is consistent with the size and sign of the bias evident in Figure 3.3. Pair-wise comparison of the notches on the boxes suggests that there is a noticeable difference between the medians from month to month.
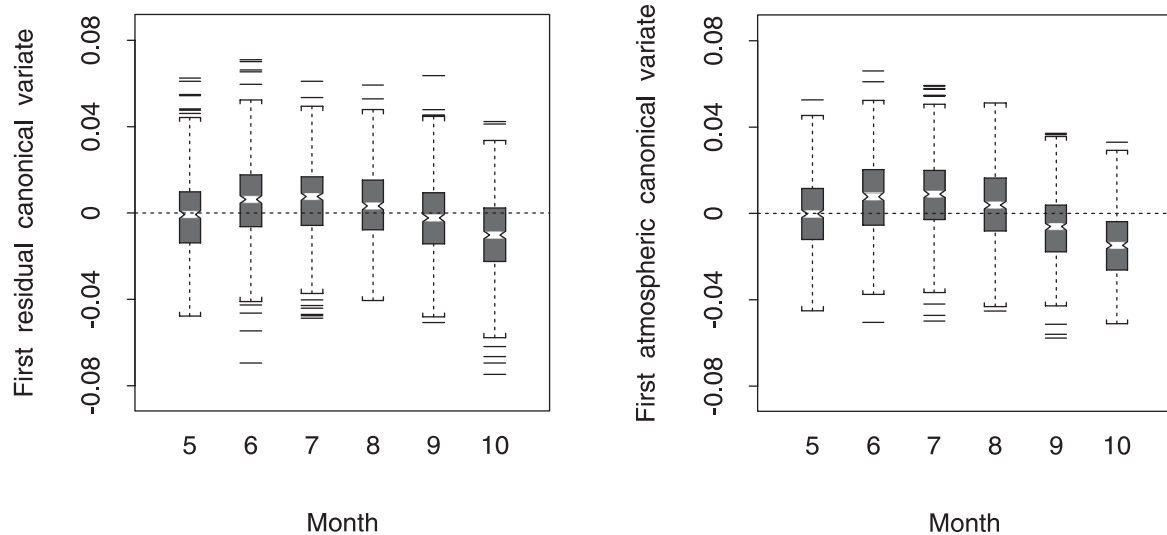
Figure 3.6   **Box plots of the first canonical variables grouped according to calendar month.**

Table 3.1 summarises the features of the scatter plots of the first atmospheric and residual canonical variables (y- and x-axes, respectively) for each weather state. For a given weather state, concentration of the values of these variables in a particular quadrant of the scatter plot indicates that the variables contain information about the occurrence of that state. Consider the columns of Table 3.1. Of the 362 data points in the 1st quadrant (upper left-hand side), 88% correspond to days assigned to States 3 to 6, and 61% to days assigned to States 4 and 5. These percentages are well above the percentage that would have been if all of the data points in the 1st quadrant had been distributed uniformly across the six weather states (i.e., 17% per state). Similarly, 88% of the 993 data points in the 2nd quadrant (upper right-hand side) correspond to days assigned to States 1, 2, 3, and 5 and 65% to days assigned to States 2 and 5. About 71% of the 401 data points in the 3rd quadrant (lower right-hand side) correspond to days assigned to States 2, 3 and 5. Also, 93% of the 1004 data points in the 4th quadrant (lower left-hand side) are correspond to days assigned to States 3 to 6, and 81% to days assigned to States 4, 5 and 6. Now consider the rows of Table 3.1. About 51% of the data points assigned to State 1 and 71% of the data points assigned to State 2 are located in the 2nd quadrant. About 53% of the data points assigned to State 4 and 70% of the data points assigned to State 6 are located in the 4th quadrant. These percentages are well above the percentage that would have been if all of the data points in a given weather state had been distributed uniformly across the quadrants (i.e., 25% per quadrant). Finally, consider positive values of the first atmospheric canonical variable alone. About 60%, 76%, 47%, 36%, 48%, and 25% of the data points for States 1 to 6, respectively, fall in the 1st and 2nd quadrants.

Thus the first atmospheric canonical variable captures information about the occurrences of States 2, 6 and, to a lesser extent, State 4.

Table 3.1 **Numbers of Data Points in Quadrants of the Scatter Plots of the First Canonical Variables for Each Weather State in the Modified NHMM.**

Weather State	Quadrant				Subtotal
	1st	2nd	3rd	4th	
1	16	90	38	34	178
2	29	385	94	38	546
3	46	137	86	121	390
4	113	90	59	297	559
5	106	264	106	290	766
6	52	27	18	224	321
Total	362	993	401	1004	2760*

* (1992-1978+1) (31+30+31+31+30+31) = 2760.

3.3   Modification of the NHMM

The results described in section 3.2 suggest the incorporation of the first atmospheric canonical variable into the predictor set for the NHMM. A stepwise regression analysis and an analysis of all-subset regressions based on leaps and bounds were undertaken to see whether a small subset of the 24 atmospheric variables could capture most of the information in the first precipitation canonical variable. This did not prove to be the case. Consequently, a NHMM with four atmospheric predictors (the fourth being the first atmospheric canonical variable) was fit to the observed atmospheric and precipitation data for 1978-92. The precipitation occurrence patterns and the composite MSLP fields associated with the weather states for the modified NHMM are almost identical to those given in Figure 3.1 and will not be given here for the sake of brevity.

Figure 3.7 compares the daily precipitation occurrence probabilities simulated by the modified NHMM with historical values for each month in the winter half-year over the period 1978-1992. Comparison of Figures 3.2 and 3.7 reveals a noticeable improvement in model fit, particularly for the months of June and July (the wettest months of the year) and October (the driest month of the winter half-year).
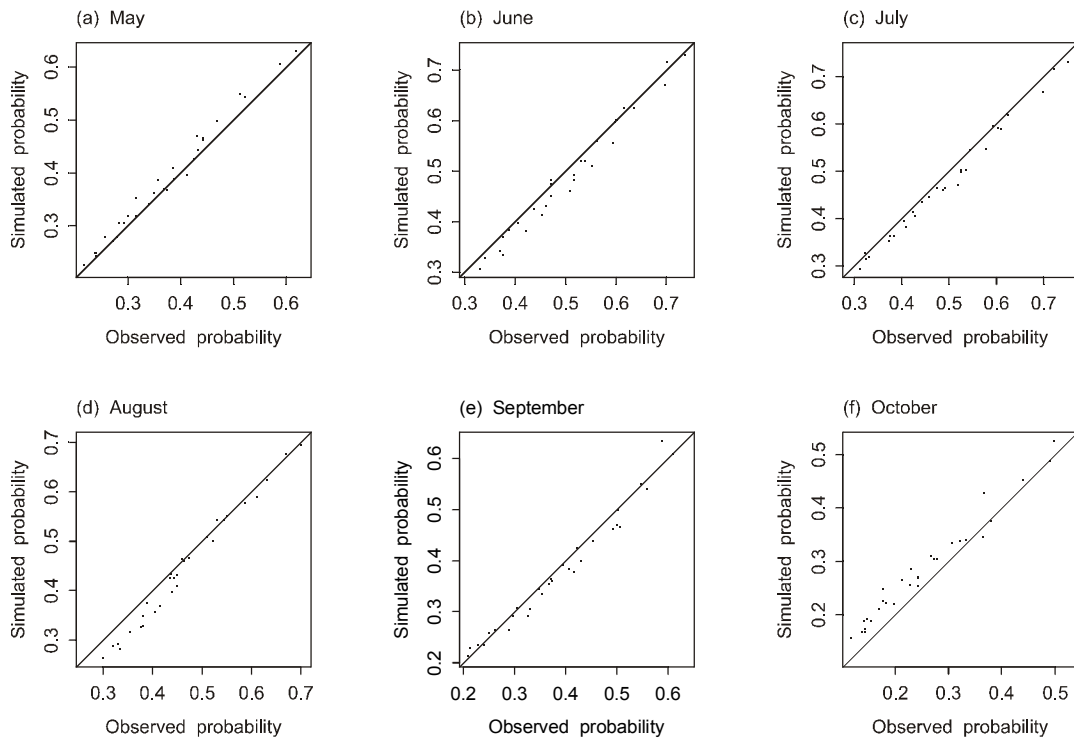
Figure 3.7 **Comparison of simulated and historical daily precipitation probabilities for the period 1978–1992 (modified NHMM).**

The seasonal distribution of the errors in the simulation of monthly precipitation amounts for Pingelly is given in Figure 3.8. Comparison of Figures 3.3 and 3.8 reveals a noticeable improvement in fit for the months of June, July, October, and perhaps September.
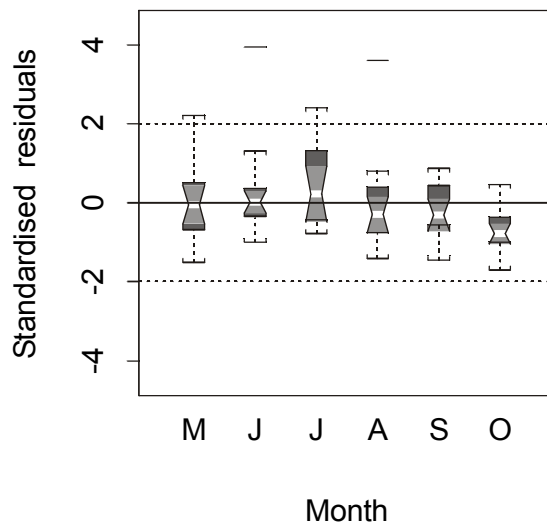
Figure 3.8 **Box plots showing seasonal distribution of standardised residuals for Pingelly (Station 28) for the period 1978–1992 (modified NHMM).**

The seasonal distribution of the monthly standardised residuals for Pingelly for the test period 1958 to 1977 is given in Figure 3.9. (Recall from section 3.2 that data for this period were not used to fit the NHMM.) The residuals exhibit a cyclical variation through the winter half-year. However the line $e = 0$ lies between the upper and lower quartiles in each case. With the exceptions of July and August, the distributions of the residuals are not symmetrical about the median in their middle regions (25th to 75th percentiles), and other diagnostics such as quantile-quantile plots (not shown) indicate departures from normality. The distribution for July contains an apparent outlier $(e = 4.02)$. Little evidence of serial correlation was found in the residuals. Consequently, we used the Wilcoxon signed-rank statistic to test the null hypothesis that the mean of the standardised residuals for a given month is zero against the alternative hypothesis that the mean is not zero. The test statistics for the months May to October were found to be significant at the 0.189, 0.011, 0.185, 1.00, 0.575, and 0.105 levels. Thus there is little evidence against the null hypothesis for all months other than June for which there is some evidence against the null hypothesis.
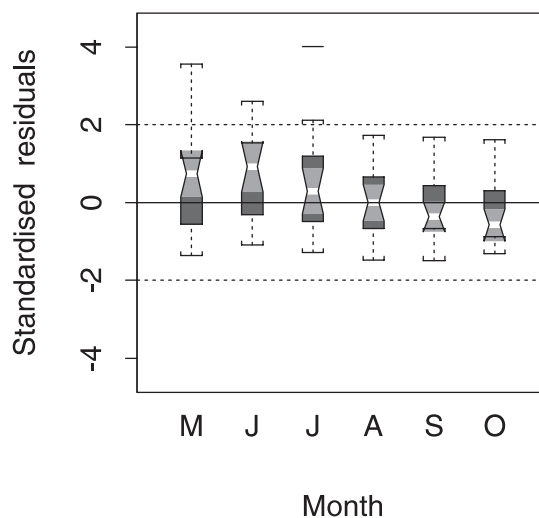
Figure 3.9   Box plots showing seasonal distribution of standardised residuals for Pingelly (Station 28) for the period 1958–1977 (modified NHMM).

A time series plot of monthly standardised residuals for Pingelly for the period 1958 to 1998 is given in Figure 3.10. Overall, the residuals form a horizontal band of uniform height centred about the line $e = 0$, and 3% of the standardised residuals lie outside of the interval $-2 \leq e \leq 2$. Similar plots have been obtained for the remaining 29 stations. All stations have monthly standardised residuals greater than 3, but these residuals comprise only 1.3% of the 30*6*41=14760 station-months and do not exhibit any temporal trends. This suggests

that the atmospheric predictors in the modified NHMM have accounted for any long-term time effects (such as changes in the atmospheric circulation over SWA) that are inherent in the Reanalysis data. Given that the period 1958 to 1977 was wet relative to 1979 to 1992, this suggests that the modified NHMM is robust against the effects of climate shifts and trends on precipitation over SWA.
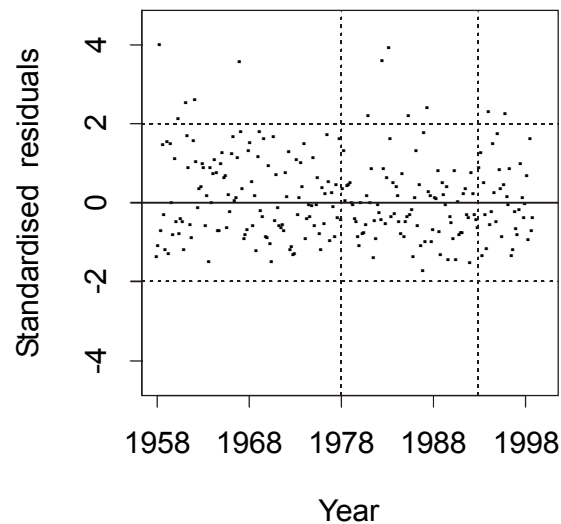
Figure 3.10   Monthly standardized residual series for Pingelly (Station 28) for the period 1958–1998 (modified NHMM). Broken vertical lines denote the fitting period for the NHMM (1978 to 1992).

4. EXPLANATION FOR THE MULTIDECADAL, WINTER PRECIPITATION DECLINE OVER SOUTHWEST AUSTRALIA

4.1 Introduction

The overall decline in annual precipitation over SWA since around the middle of the 20th century has been the subject of much interest [see citations in IOCI (1999) and Tapp and Cramb (2000)]. Most of the decrease is evident in the winter half-year (May-October) when about 80 percent of the annual precipitation occurs. The number of rain days in the winter half-year has decreased over much of the region, and the average intensity and frequency of rare high-precipitation events during that season have decreased.

The winter precipitation decline has had a marked effect on the surface water resources of the Perth region over the last 25 years. Figure 4.1 shows a bar chart of the total annual inflow for the major reservoirs in the Perth water supply system. The water year is defined by the period from May to April. Since the 1975 water year, dam inflows have been consistently smaller than those in the past and, with only one exception (1996), smaller than the long term mean annual inflow. Only once has an annual total precipitation at Perth exceeded the 70th percentile since 1967 (Tapp and Cramb, 2000).
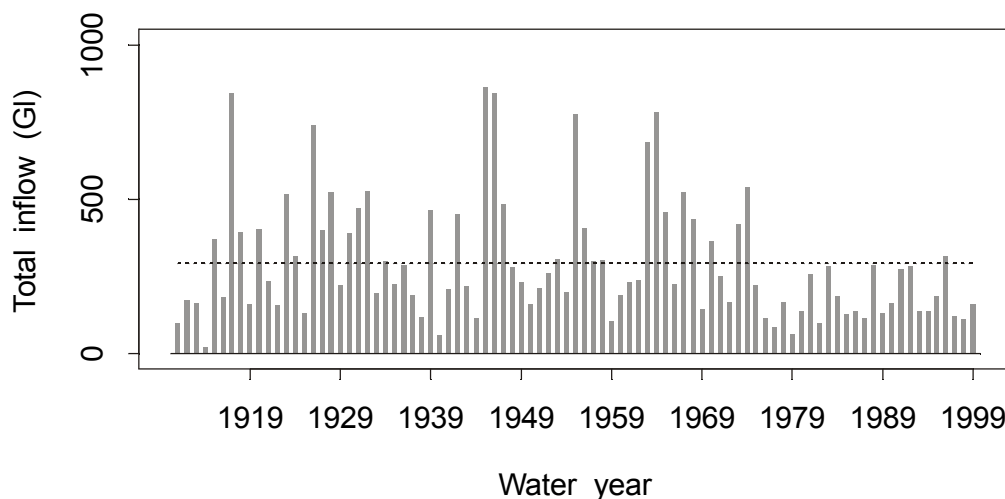
Figure 4.1   Annual inflow series for major surface water sources, Perth Water Supply System. Dashed line shows mean annual inflow for complete record. (Series supplied by Water Corporation of Western Australia.)

The timing of the abrupt shift in the inflow series roughly coincides with changes to the frequency characteristics of El Niño and a marked warming in the Indian Ocean after 1976 (see citations in Clark *et al.,* 2000). Since 1975, El Niños are twice as frequent as La Niñas. This suggests that an investigation of the atmospheric circulation over SWA for the period covered by the Reanalysis dataset (1958-1998) could be revealing.

4.2   Approach

The linkage between the winter precipitation decline and regional changes in atmospheric circulation are investigated using the NCEP-NCAR Reanalysis dataset, observed daily precipitation series for the 30 sites shown in Figure 2.1, and the modified nonhomogeneous hidden Markov model (NHMM) described in section 3. Recall that the transition from a given weather state to another in the NHMM is conditioned on a relatively small number of atmospheric variables (predictors) derived from the Reanalysis dataset. Thus any changes in the evolution of the weather states may be linked to temporal changes in the atmospheric predictors.

We hypothesized that the recent precipitation decline in SWA was caused by a change in the atmospheric circulation that occurred around 1976; and that this change would manifest itself in both the atmospheric predictor series used to condition the weather state transition probabilities in the NHMM and the weather state sequence derived from the fitted NHMM.

We split the atmospheric predictor series and the weather state sequence into two parts with the breakpoint occurring at October 31st in either 1974, 1975, 1976, 1977, or 1978. These breakpoints encompass the large-scale climate shift that occurred around 1976. The periods from 1958 to the breakpoint year, and the year following the breakpoint to 1998, are hereafter called Epoch 1 and Epoch 2.

Our analysis consisted of three parts:

(1)   Comparison of the NHMM weather state sequence for 1958 to the mid–70s with that for the mid–70s to 1998. The comparison was made on a winter and a calendar month basis. Plots of weather state probability series were used to discern any changes in synoptic patterns that may have occurred prior to the mid-70s.

(2)   An exploratory data analysis comparing the atmospheric predictor series for Epoch 2 with that of Epoch 1.

(3)   A sensitivity analysis to investigate whether the precipitation decline since the mid–70s can be attributed to changes in the behaviour of a single predictor in the NHMM.

4.3   Methods

4.3.1   Analysis of Weather State Sequence

a.   Changes in steady-state probabilities of weather states

We used a two-sample *t*-test to assess the statistical significance of differences between the means of the winter weather state probability series for Epochs 1 and 2. Exploratory analyses indicated that the data did not exhibit significant autocorrelation or departures from normality. Rather than set an essentially arbitrary significance level, we used the probability value (*P*-value) to measure the strength of the evidence against the null hypothesis that the means are equal. The *P*-value is the probability that a test statistic at least as extreme as that observed could have arisen by chance.

b.   Changes in weather state counts for each calendar month in winter

When the sampling interval is reduced from six months to one month, the number of occurrences of any given weather state is relatively low. Therefore, it is more appropriate to consider weather state counts (a discrete random variable) rather than weather state probability (a continuous random variable). Given that weather state counts series are discrete, we used lag plots to check for serial correlation in the counts series for each period: little evidence of serial correlation was found. An exploratory analysis of the counts data indicated that the underlying probability distributions were multimodal. This precluded inferences based on commonly used discrete probability distributions. Consequently, we used randomization to test the hypothesis that average weather state counts for Epoch 2 are the same as those for Epoch 1. That is, to test whether the observed counts series for the weather states are likely or unlikely to have arisen by chance.

Randomization testing is a procedure that is less dependent on distributional assumptions than conventional statistical methods. It involves the determination of the *P*-value of a test statistic computed for an observed dataset by comparing the statistic's value with the

distribution of values obtained by calculating the test statistics for a large number of re-orderings of the data (Manly, 1991). Here the *P*-value is the proportion of values that are as extreme or more extreme than the test statistic's value in the randomization distribution.

Box plots of the weather state counts data indicated the presence of extreme sample values and long-tailed probability distributions in several instances. Thus the sample mean would be a poor estimator of location. For each calendar month *m* and weather state *s* we test for a difference between the median weather state counts for Epochs 1 and 2. The test statistic is defined by

$$\widetilde{c}_{ms} \; = \; \widetilde{c}_{1ms} \; - \; \widetilde{c}_{2ms} \tag{4}$$

where $\widetilde{c}_{1ms}$ and $\widetilde{c}_{2ms}$ are the median counts for weather state *s* in Epochs 1 and 2, respectively. We used two-sided tests throughout since marked increases or decreases in weather states counts across the two epochs are of interest. Thus large positive and large negative values of $\widetilde{c}_{ms}$ are regarded as evidence against the null hypothesis that the medians are equal. We used 5000 randomizations for each *m* and *s* pair in (4) since complete enumeration of all possibilities would require an impractical $41!/20!(41-20)! \approx 10^{12}$ re-orderings of the observed dataset.

c.   *Changes in weather state transition probabilities*

The application of 6×6=36 univariate two-sample *t*-tests to the components of weather state transition probability matrices could lead to the possibility of obtaining a significant result by chance alone. Therefore, we used the Hotelling two-sample T^2-test. Let *N* denote the number of weather states and $\mathbf{X}^i$, $(i = 1, \cdots, N)$, denote a transition probability matrix with elements:

$$x_{\tau j}^i \; = \; \overline{P(S_j \mid S_i)}_\tau; \quad j = 1, \cdots, N-1, \quad \tau = 1, \cdots, n \tag{5}$$

where $\overline{P(S_j \mid S_i)}_\tau$ denotes the estimated one-step transition probability of going from weather state *i* on one day to weather state *j* on the next day during year τ. The probability $\overline{P(S_N \mid S_i)}_\tau$ is ignored since

$$\overline{P(S_N \mid S_i)}_\tau = 1 - \sum_{j=1}^{N-1} x_{ij}^i \tag{6}$$

We used the Hotelling two-sample T^2-statistic to test the null hypothesis that the population mean vectors of the transition probability matrices for both Epochs are identical against the alternative hypothesis of different means (Chatfield and Collins, 1980). Let $\mathbf{X}_1^i$ and $\mathbf{X}_2^i$ denote the matrices defined by (5) for the pre-1978 and post-1978 periods, respectively. The T^2-statistic is defined by

$$T^2 = \frac{n_1 n_2}{n_1 + n_2} (\overline{\mathbf{x}}_1^i - \overline{\mathbf{x}}_2^i)^T \mathbf{S}^{-1} (\overline{\mathbf{x}}_1^i - \overline{\mathbf{x}}_2^i) \tag{7}$$

where $\overline{\mathbf{x}}_1^i$ and $\overline{\mathbf{x}}_2^i$ denote the column means of $\mathbf{X}_1^i$ and $\mathbf{X}_2^i$, the superscript T denotes the transpose of a vector or matrix, and $\mathbf{S}$ denotes the pooled estimate of the common covariance matrix:

$$\mathbf{S} = \frac{(n_1 - 1)\mathbf{S}_1 + (n_2 - 1)\mathbf{S}_2}{n_1 + n_2 - 2} \tag{8}$$

in which $\mathbf{S}_1$ and $\mathbf{S}_2$ denote the sample covariance matrices of $\mathbf{X}_1^i$ and $\mathbf{X}_2^i$. The statistic

$$F = \frac{n_1 + n_2 - p - 1}{(n_1 + n_2 - 2)p} T^2 \tag{9}$$

has the variance ratio F distribution with degrees of freedom p and $n_1 + n_2 - p - 1$.

The T^2-distribution is a multivariate generalization of the Student t-distribution. Thus the T^2-test assumes that the transition probability matrices have a multivariate normal distribution with the same, though unknown, covariance matrix. Although the T^2-statistic is not sensitive to the assumption of equal covariance matrices when the sample sizes are approximately equal, severe departures from normality may be cause for concern. Consequently, we used randomization tests with 5000 randomizations each to check the P-values of the T^2-statistics computed from the observed transition probability matrices.

4.3.2   Exploratory Analysis of Atmospheric Predictor Series

The exploratory analysis focused on comparisons of the probability distributions of the predictors for Epochs 1 with those for Epoch 2. The analysis consisted of two plots for each predictor: a Tukey mean-difference (m-d) plot (Cleveland, 1993); and a plot of the smoothed density estimates (Venables and Ripley, 1994) for each Epoch. Let E_{1p} and E_{2p} denote the pth quantile for a given predictor for Epochs 1 and 2, respectively. (The pth quantile is the value of the predictor below which $100p$ of the values fall.) The m-d plot graphs the differences $E_{1p} - E_{2p}$ against the means $(E_{1p} + E_{2p})/2$. Thus the differences will be zero if the empirical distributions for Epochs 1 and 2 are the same, while systematic deviations from the zero difference line indicate the nature and size of differences between the distributions. Density estimates can give valuable indications of features such as skewness and multimodality in data. The oldest density estimator for univariate data is the histogram. However, the interpretation of the features in a histogram is sensitive to the choice of the number of class intervals and starting point of the class intervals. We used *kernel density* smoothers instead.

4.3.3   Sensitivity Analysis

The atmospheric predictors enter the NHMM in a nonlinear fashion. Therefore, it is difficult to discern whether the low precipitation sequence is due to changes in one atmospheric predictor alone or a combination of predictors. We assessed the impact of a change in the distribution of any one of the three key predictors (mean MSLP, north-south MSLP gradient and DT_d^{850}) by transforming its pre-1978 distribution to its post-1978 distribution. For a given key predictor x, the transformation is described by $x_2 = F_{X_2}^{-1}(F_{X_1}(x_1))$ where x_1 and x_2 denote Epochs 1 and 2, and $F_{X_i}()$, $i = 1, 2$, denotes the cumulative distribution function for the ith Epoch. The transformed values of the fourth predictor (i.e., first atmospheric canonical variable) were determined using the x_2 values and the pre-1978 values for the remaining 23 predictors. One-thousand, 20-year sequences of daily winter precipitation were generated from the fitted NHMM, conditionally on the 20-year sequence for each transformed atmospheric predictor with the pre-1978 distributions for the remaining key predictors left unchanged. The statistics of the simulated weather state and precipitation sequences obtained were then compared with those obtained from simulations driven by the post-1978 data.

4.4 Results

4.4.1 Analysis of Weather State Sequence

Table 4.1 reports the results of the two-sample, two-sided *t*-tests for the steady-state probability series for States 3 and 5. There is very strong evidence against the null hypothesis for State 3, and the strength of the evidence is insensitive to breakpoint selection. Some sensitivity to breakpoint selection is evident for State 5. Nevertheless, the strength of the evidence against the null hypothesis is strong to very strong. For States 1, 2, 4, and 6, the *P*-values lie in the interval $0.087 \leq P\text{-value} \leq 0.798$. Thus there is little evidence against the null hypothesis for these states.

Table 4.1   Comparison of mean probabilities of States 3 and 5 for Epochs 1 and 2.

Breakpoint	State 3		State 5	
	t-statistic	*P*-value	*t*-statistic	*P*-value
1974	5.313	4.64×10^{-6}	-4.182	1.58×10^{-4}
1975	5.240	5.86×10^{-6}	-3.621	8.35×10^{-4}
1976	5.024	1.16×10^{-6}	-3.654	7.58×10^{-4}
1977	4.488	6.21×10^{-5}	-3.296	0.002
1978	4.158	1.70×10^{-4}	-2.905	0.006

Table 4.2 reports the results of the randomization tests for monthly weather state counts for States 3 and 5. Some sensitivity to breakpoint selection is evident. However, for July and August there is strong evidence against the null hypothesis that mean State 3 counts for Epoch 2 are the same as those for Epoch 1. October is the only month for which the evidence against this null hypothesis is weak. For May to August, there is some to very strong evidence against the null hypothesis that mean State 5 counts for Epoch 2 are the same as those for Epoch 1.

Table 4.3 reports the results of the Hotelling two-sample T^2-tests for the weather state transition probability matrices for States 2, 3 and 5. (For States 1, 4 and 6 there is little evidence against the null hypothesis that the population mean vectors of the transition probability matrices for both Epochs are identical.) The *P*-values obtained using the distributional assumption about the transition probability matrices and randomization are in essential agreement, and are fairly insensitive to breakpoint selection. For transitions *from* State 2 there is very strong evidence against the null hypothesis that the population mean

vectors for both Epochs are identical. Inspection of time series plots of $\overline{P(S_3 \mid S_2)}$ and

$\overline{P(S_4 \mid S_2)}$ for 1958-1998 revealed underlying decreasing and increasing trends, respectively. Thus the corresponding means for Epochs 1 and 2 are quite different. In contrast, there is little evidence that the transition probabilities from any state *to* State 2 have changed. For transitions *from* State 3 there is strong to very strong evidence against the null hypothesis. The mean $\overline{P(S_3 \mid S_3)}$ for Epoch 2 is lower than that for Epoch 1, while the mean $\overline{P(S_5 \mid S_3)}$ for Epoch 2 is noticeably higher than that for Epoch 1. These findings provide further insight into the change in frequency of State 3 in that the day-to-day persistence of State 3 has decreased and the frequency of the transition from State 3 to dry conditions region-wide (State 5) have increased during 1958-1998. The *P*-values for transitions *to* State 3 are sensitive to breakpoint selection, and the level of evidence against the null hypothesis ranges from little to strong. There is little evidence against the null hypothesis that the probabilities of transitions *from* State 5 *to* any other state or the same state have not changed. However, for transitions *to* State 5 there is strong evidence against the null hypothesis: for Epoch 2 the $\overline{P(S_5 \mid S_j)}, \; j = 1, \ldots, 6,$ are higher than those for Epoch 1.

Table 4.2   **P-values from randomization tests on monthly weather state counts for States 3 and 5.**

Break-	Winter Month					
point	**May**	**June**	**July**	**August**	**September**	**October**
	State 3					
1974	0.016	0.002	0.002	0.002	0.013	0.109
1975	0.012	3×10^{-4}	0.003	0.002	0.003	0.024
1976	0.015	0.013	0.002	0.002	0.003	0.054
1977	0.015	0.008	0.006	0.004	0.012	0.073
1978	0.011	0.010	0.004	0.007	0.003	0.050
	State 5					
1974	0.002	1×10^{-4}	1×10^{-4}	0.011	1×10^{-4}	0.007
1975	0.006	0.002	1×10^{-4}	0.014	0.033	0.018
1976	0.016	0.004	1×10^{-4}	0.014	0.055	0.016
1977	0.014	0.011	0.014	0.016	0.122	0.036
1978	0.007	0.046	0.024	0.012	0.209	0.209

Table 4.3   **Results of Hotelling two-sample T^2-tests comparing the mean weather state transition probabilities for Epochs 1 and 2.**

Weather	Transition From State S		Transition to State S	
State, S	F statistic	P-value*	F statistic	P-value*
1974				
2	7.754	0.0001	1.834	0.124
3	5.363	0.0009	3.838	0.0054
5	0.632	0.677	4.123	0.0035
1975				
2	6.828	0.0002	1.691	0.155
3	4.199	0.0043	4.016	0.0041
5	0.471	0.795	3.892	0.0050
1976				
2	6.081	0.0004	2.058	0.0864
3	5.294	0.0010	3.096	0.0166
5	0.888	0.500	4.570	0.0019
1977				
2	8.246	< 0.0001	1.403	0.244
3	4.000	0.0056	2.822	0.0256
5	0.590	0.708	3.736	0.0063
1978				
2	8.823	< 0.0001	1.226	0.319
3	3.536	0.011	2.263	0.0622
5	0.503	0.772	4.311	0.0027

* *P*-values based on the assumption that transition probability matrices have a multivariate normal distribution.

Although the above results *may* seem to be inconsistent with those reported in Table 4.1, the relationship between the steady state and transition probabilities is described by the following system of equations:

$$P(S_i) = \sum_{k=1}^{N} P(S_k)\, P(S_i \mid S_k), \quad i = 1, \cdots, N$$

$$\sum_{i=1}^{N} P(S_i) = 1 \tag{10}$$

Hence $P(S_i)$ is a nonlinear function of the components of the ith column of the transition probability matrix, and the effects of changes in these transition probabilities on the steady state probability will not take a simple form.

Plots of the winter weather state probability series for states 3 and 5 are given in Figure 4.2. Although interannual variability is evident in both plots across the 1958-98 period, it is apparent that the frequency of State 3 declined from 1958 to the mid–70s and has remained stationary since that time (Figure 4.2a). In contrast, the frequency of State 5 increased abruptly around the early to mid–70s (Figure 4.2b) and has remained stationary since the apparent break. Consider the precipitation occurrence patterns and corresponding composited MSLP fields for States 3 and 5 given in Figure 3.1. If kinks in the isobars of low pressure systems in MSLP charts can be interpreted as indicative of the presence of cold fronts (Sturman and Tapper, 1996, p. 171), a reduction in the frequency of State 3 indicates a reduction in the occurrence of post-frontal rainfall. An increase in the frequency of State 5 indicates a decrease in the number of rain days across SWA. This is due to an increase in the frequency of dry easterly or northeast winds around high pressure systems centred to the east of the region.
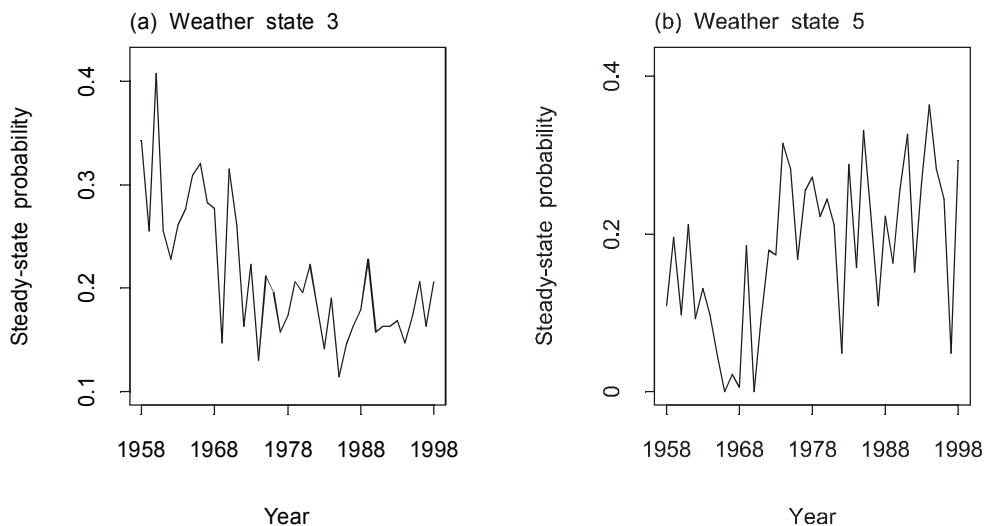
Figure 4.2   **Interannual variability of steady-state probabilities for weather states 3 and 5.**

The underlying shift and trend evident in Figure 4.2 suggest that the observed low precipitation sequence is due to climate forcing by at least two large-scale and possibly interacting mechanisms. The mid-70s break in the probability series for States 3 and 5 roughly coincides with the timing of the observed change in the behaviour of El Niño (see section 4.1). The presence of high pressure systems in the Australian region is more pronounced during El Niño episodes, and the change in the frequency of State 5 is consistent with the decline in the number of La Niña episodes relative to El Niños. The decline in the

frequency of State 3 may be linked to a change in the behaviour of the Antarctic Oscillation. One index of the Oscillation is the first empirical orthogonal function (EOF) of sea level pressure (SLP) for the latitudinal band between 20 and 60º S. Figure 4.3(a) depicts the SLP anomaly when the index is positive; a region of lower than usual SLP surrounds the Antarctic continent while regions of higher than usual SLP occur at middle latitudes. Under these conditions, westerly airflow in the mid latitudes is suppressed. Figure 4.3(b) shows the index time series derived from the Reanalysis record by CAR. The index is negative in sign prior to the mid-70s, and positive thereafter. Also, the index increases from high negative values in the early 1960s to positive values in the late 1970s.

Inspection of Figure 3.1 suggests that States 2 and 4 also involve southwest to westerly airflow. As noted above, the mean transition probabilities *from* State 2 for Epoch 2 are different to those for Epoch 1. Comparison of the composite MSLP plots for States 2 and 3 suggests that both conform to the typical pattern of a trough between two anticyclones that is conducive to the development of cold fronts. Fronts separate two air masses of contrasting wind, temperature and density, and in the Australian region are largely due to the interaction of subtropical and polar air. These features are not as apparent in the composite MSLP plot for State 4. State 4 appears to be indicative of weak frontal systems, or frontal systems that are centred too far south to penetrate the hinterland. Recall that no significant change in the steady-state or transition probabilities for State 4 was detected. Overall, these results suggest that the hypothesised linkages between the low precipitation sequence and changes in the behaviour of El Niño and the Antarctic Oscillation need to be subjected to a detailed meteorological analysis.

4.4.2 Exploratory Analysis of Atmospheric Predictor Series

Figure 4.4 shows mean-difference and smoothed density plots for the key atmospheric predictors when Epochs 1 and 2 are defined as the periods 1958–76 and 1977–98, respectively. The post-1976 changes in the probability distributions of the predictors differ from each other. The MSLPs for Epoch 2 are roughly equal to MSLPs for Epoch 1 plus a constant of 0.6 hPa. The spread of N-S MSLP gradient for Epoch 2 is marginally larger than that for Epoch 1. The distribution of DT_d^{850} values for Epoch 2 has a longer upper tail than that for Epoch 1. This suggests that when the lower troposphere is dry, it is much drier in Epoch 2 than in Epoch 1.

(a)

(b)
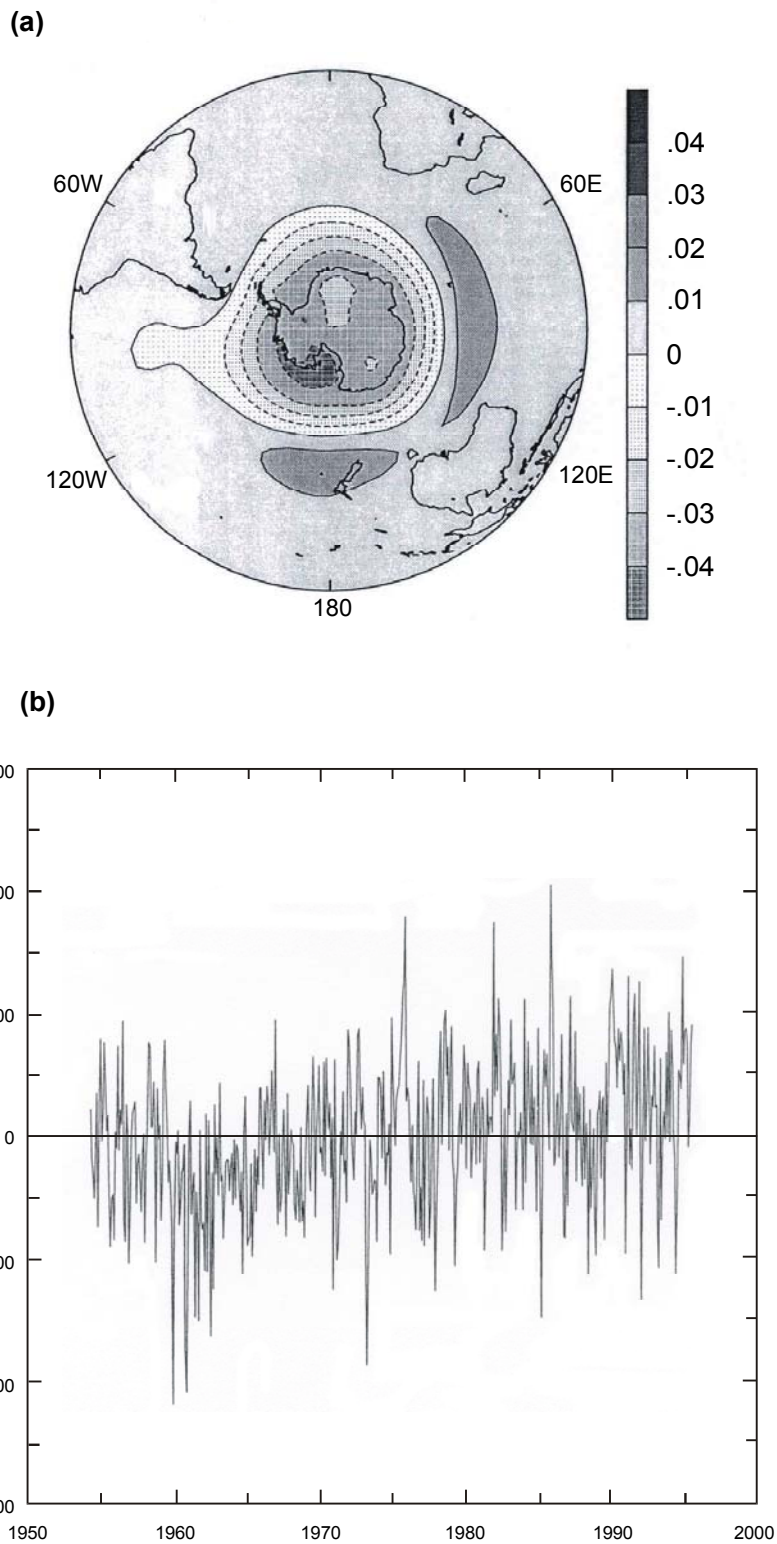
Figure 4.3 **Antarctic Oscillation: (a) pressure anomaly when the first EOF of sea level pressure is positive, (b) time series of the first EOF. (Source: Peter Whetton, CSIRO Atmospheric Research.)**
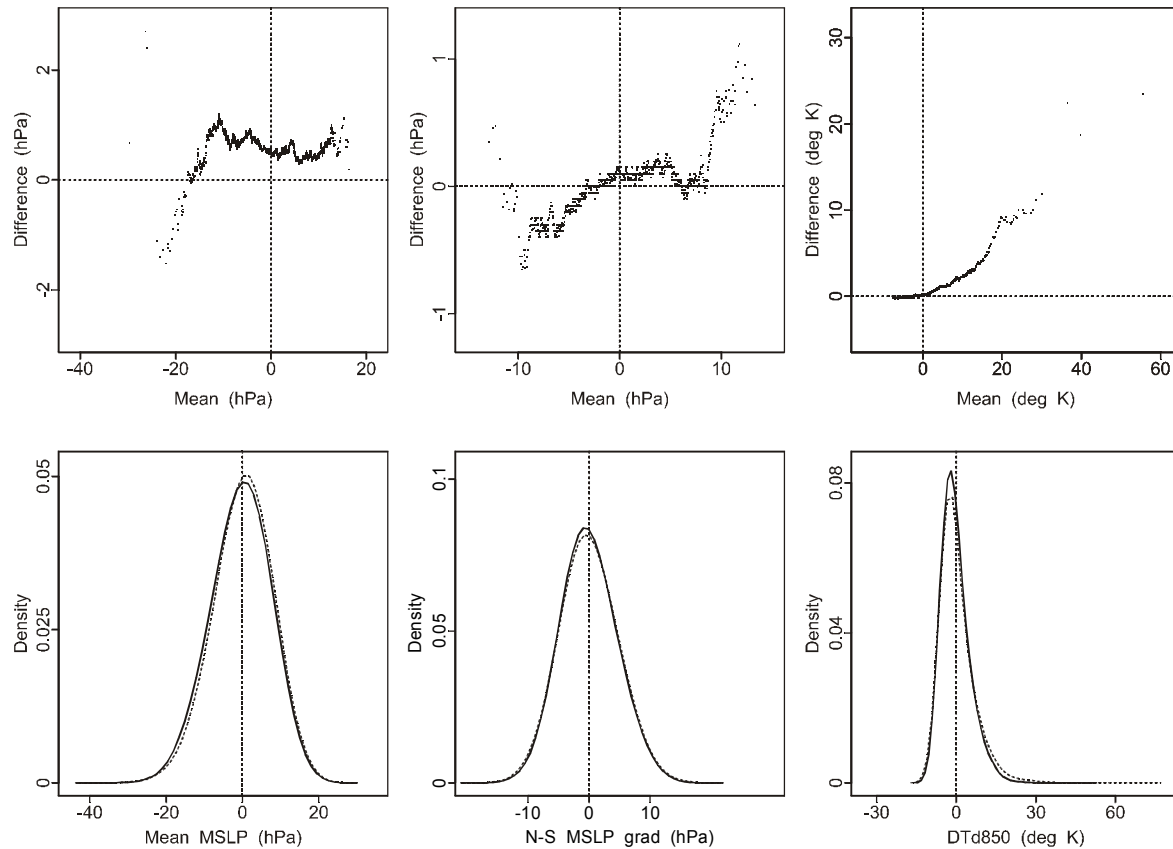
Figure 4.4   Mean-difference plots and smoothed density estimates of centred, NHMM atmospheric predictor series for the periods 1958–76 (Epoch 1) versus 1977–98 (Epoch 2). In each density plot the density estimates for 1977-1998 are shown as dotted curves.

4.4.3   Sensitivity Analysis

Results from the sensitivity analysis are given in Figure 4.5. The probability residuals for a particular weather state are defined herein as the difference between the 'observed' steady state probabilities for each year in the 1979-1998 period and the mean of the 1000 simulated probabilities for each year. The raindays residuals are defined as the difference between the observed mean values of the number of raindays at each site for 1979-1998 and their simulated means. The rainfall residuals are defined as the difference between the observed mean values of rainfall amounts at each site for 1979-1998 and their simulated means.

Perusal of Figure 4.5 indicates that post-1978 changes in any one of the three predictors alone cannot explain the decline in the frequency of State 3 nor the number of rain days over SWA (Figures 4.5a and 4.5c). In contrast, the increase in the frequency of State 5 can be explained by changes in any one of the three predictors (Figure 4.5b). The results for mean winter

precipitation (Figure 4.5d) are not informative given that the NHMM simulations based on the 1979-98 Reanalysis data are slightly biased. Nevertheless, it is apparent that the changes in weather state frequency and precipitation across SWA are due to changes in a combination of atmospheric predictors rather than a single predictor.
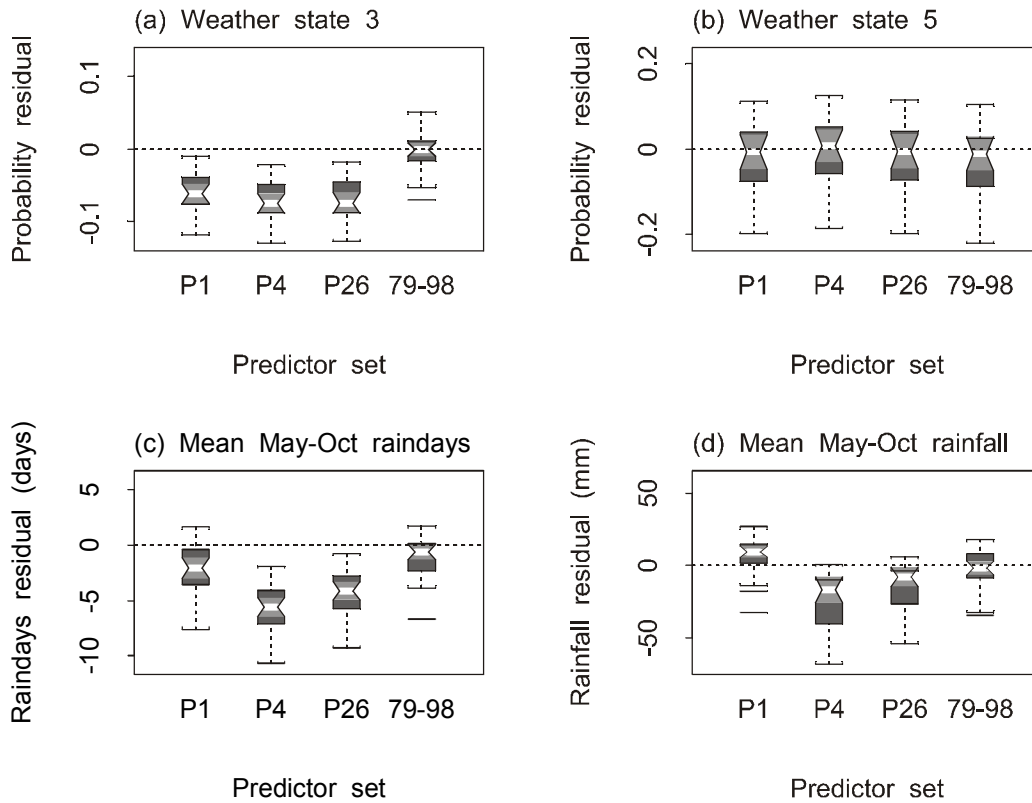
Figure 4.5　　**Box plots of results from sensitivity analysis: (a) and (b) show differences between observed and mean simulated weather state probabilities, (c) shows differences between mean observed rain days and mean simulated rain days for all 30 sites, and (d) shows the relative percentage error in mean simulated precipitation across the 30 sites. P1, P4 and P26 denote results for transformed mean MSLP, north-south MSLP gradient and DT_d^{850}, respectively, and 79-98 denotes results when the post-1978 data for all predictors are used to drive the modified NHMM.**

4.5　　Discussion

Other workers have investigated the causes of the low precipitation sequence over SWA. Allan and Haylock (1993) found that wet and dry periods over most of the region are associated with enhanced and weaker mean westerly airflow, respectively. Smith *et al*. (1999) noted an increase in winter MSLPs over SWA since the late 1960s and a decrease in cyclonic activity immediately south of WA over the same period. Our results are consistent with these earlier findings in that comparing the last twenty years (Epoch 2) with the previous twenty years (Epoch 1):

- Winter MSLP for Epoch 2 is equal to that for Epoch 1 plus an additive shift of 0.6 hPa (Figure 4.4).

- There has been a significant reduction in the number of days when precipitation is generated by westerly airflow (Figures 3.1a and 4.2).

- There has been a significant increase in anticyclone activity (Figures 3.1b and 4.2).

Tapp and Cramb (2000) have speculated that changes in atmospheric circulation that are not well reflected by changes in MSLP may also affect regional precipitation. We have found that when the lower troposphere has been dry in Epoch 2, there is a tendency for it to have been drier than in Epoch 1 (Figure 4.4). We have also demonstrated that the low precipitation sequence is due to a combination of changes in sea level pressure and low-level humidity variables rather than a single pressure variable alone (Figure 4.5).

4.6   Conclusions

Our results indicate that:

- There is strong to very strong evidence of changes in the synoptic patterns over SWA during the last 40 years.

- There are marked reductions in the incidence of precipitation generated by moist westerly and south-west winds, and the number of rain days due to an increase in the frequency of high pressure systems centred to the east of SWA.

- The changes in weather state frequency, and hence precipitation occurrence and amount, are due to a combination of changes in several atmospheric variables (mean MSLP, north-south MSLP gradient and DT_d^{850}) rather than any one predictor.

We have *speculated* that the large-scale mechanisms responsible for the low precipitation sequence may be changes in, and a possible interaction between, the behaviour of El Niño and the Antarctic Oscillation over the period covered by the Reanalysis dataset. This hypothesis should be subjected to detailed meteorological analysis.

5.   LOW FREQUENCY CLIMATE VARIABILITY

5.1   Introduction

Previous work by CSIRO Atmospheric Research (IOCI, 1999) has indicated that the observed low precipitation sequence for SWA is unusual in a historical and global context. In this section, we attempt to place the observed sequence in a regional context by applying the NHMM to the daily atmospheric fields produced by the 1000-year, CSIRO Mk 2 coupled GCM run. This approach produces a daily precipitation sequence of length 1000 years for each of the 30 sites in SWA (Figure 2.1 and Table 2.1).

Consider the 40-year period from 1958 to 1997. One way of characterising the recent precipitation decline over SWA is to compute the difference between the mean precipitation across all 30 sites for the period 1958 to 1977 and the mean precipitation across all 30 sites for 1978 to 1997. This difference will hereafter be referred to as the observed mean difference. We estimate the probability of a mean difference that is at least as severe as the observed as follows:

- For each of the 961 periods of length 40 years in the 1000-year GCM run, compute a simulated mean difference by subtracting the mean precipitation for the last 20 years across all 30 sites from the mean precipitation for the first twenty years.

- Collate and sort the 961 simulated mean differences.

- Compare the observed mean difference to the empirical quantiles of the distribution of the simulated mean differences.

5.2   Results and Discussion

Figure 5.1 compares the distribution of simulated mean differences with the observed mean difference (27.2 mm). About 9.5% of the simulated mean differences are greater than the observed mean difference, indicating that the observed low precipitation sequence is uncommon but not extreme.

However, the above finding is subject to three caveats:

- It assumes that the 1000-year GCM run produces a credible simulation of low-frequency changes in atmospheric circulation over SWA.

- It assumes that the parameters of the NHMM are stationary over the length of the GCM simulation.

- The GCM simulation is not a reconstruction of climate variability over the last 1000 years, as temporal variations in solar forcing, volcanism and the atmospheric concentration of carbon dioxide over that period have not been accounted for. That is, the simulation is a scenario derived for present day conditions only.
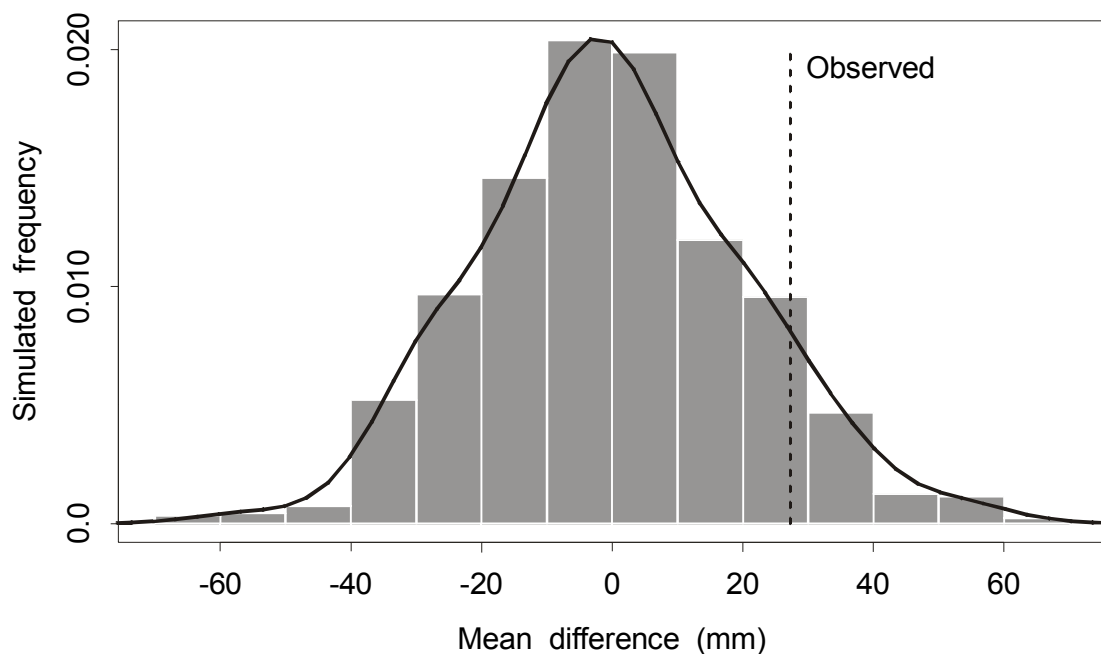

Figure 5.1   **Comparison of the observed mean difference and simulated mean differences.**

6.   CONCLUSIONS

6.1   Summary of the Investigation

Our investigations for Second Research Phase of the Indian Ocean Climate Initiative (IOCI) have focused on:

- Split-sample testing of an extended nonhomogeneous hidden Markov model (NHMM) for daily winter (May to October) precipitation across a network of 30 stations scattered throughout southwest Western Australia (SWA).

- Using the NHMM and observed atmospheric fields to discern the causes of the low precipitation sequence in SWA at the synoptic scale.

- Deriving an estimate of the probability of the observed low precipitation sequence over the last two decades.

Our main findings are as follows:

- Initial testing revealed that the NHMM did not capture the dynamic behaviour of the atmosphere at intra-seasonal time scales. A modified version of the NHMM incorporating an augmented atmospheric predictor set was shown to resolve most of the performance deficiencies of the original model. This suggests that provided coupled ocean-atmosphere GCMs could provide reasonable interseasonal forecasts of the large-scale atmospheric circulation over SWA, reasonably reliable forecasts of monthly precipitation at sites across the region can be obtained.

- A sudden change in spatial precipitation occurrence patterns occurred in the mid 70s. Changes in the location and strength of depressions and anticyclones, and the moisture content of the lower troposphere, are evident.

- The low precipitation sequence over the last 20 years is due to changes in a combination of several atmospheric variables rather than a change in any one variable.

- Within the winter half-year, the number of days when the entire southwest is essentially dry is larger than in the past due to the increase in the number of days when anticyclones

are centred to the east of the region. This *may* be due to the change in the behaviour of El Niño that occurred around 1976.

- There has been a reduction in the frequency of precipitation in coastal regions due to a reduction in westerly airflow. There is a declining trend in the frequency of this precipitation pattern from 1958 to the mid-70s, with some evidence of oscillations about the trend. The trend has been absent for the period from the mid-70s to present. This *may* be due changes in the Antarctic Oscillation and an interaction between the Oscillation and El Niño.

- In a regional context, the low precipitation sequence over the last 20 years is uncommon but not extreme.

6.2   Future Research

Our proposed research plan for Phase 5 of IOCI is as follows:

- Downscaling of a sequence of staged, interseasonal climate forecasts using CAR's coupled ocean-atmosphere GCM, and comparison of downscaled precipitation with observations. This work will reveal the lead time for reliable forecasts (if any), and any so-called 'predictability barriers' during the winter half-year.

- Further investigation of the effects of El Niño and the Antarctic Oscillation on winter precipitation over SWA.

- Development of an air temperature module for the NHMM. This module will simulate minimum daily temperature and temperature range (maximum minus minimum daily temperature).

Our proposed research linkages for Phase 5 are:

- *CSIRO Atmospheric Research* – deriving interseasonal forecasts of monthly precipitation over SWA by downscaling a staged sequence of coupled CSIRO Mark 3 GCM simulations, and obtaining further insight into the relationships between key atmospheric predictors and large-scale forcing mechanisms.

- *Bureau of Meteorology (Research Centre and Perth Regional Office)* – collaboration on the final synthesis report for policy makers.

- *University of Washington, Seattle* – consultation on strategic issues related to further development of the NHMM.

- *CSIRO Mathematical and Information Sciences* – advice on advanced statistical issues and obtaining further insight into the relationships between key atmospheric predictors and large-scale forcing mechanisms.

7.   REFERENCES

Allan, R.J. and Haylock, M.R. (1993). Circulation factors associated with the winter rainfall decrease in southwestern Australia. *J. Climate, 6,* 1356-1367.

Arnell, N., Bates, B.C., Lang, H., Magnuson, J.J. and Mulholland, P. (1996). Hydrology and freshwater ecology. In: *Climate Change 1995: Impacts, Adaptations and Mitigation of Climate Change: Scientific-Technical Analyses.* Contribution of Working Group II to the Second Assessment Report of the Intergovernmental Panel on Climate Change. R.T. Watson, M.C. Zinyowera, and R.H. Moss (ed.), Cambridge Univ. Press, Cambridge, 325-363.

Bardossy, A. and Plate, E.J. (1991). Modelling daily precipitation using a semi-Markov representation of circulation pattern occurrence. *J. Hydrol.*, 122, 33-47.

Bardossy, A. and Plate, E.J. (1992). Space-time model for daily precipitation using atmospheric circulation patterns. *Water Resour. Res., 28*(5), 1247-1259.

Bogardi, I., Matyasovszky, I., Bardossy, A. and Duckstein, L. (1993). Application of a space-time stochastic model for daily precipitation using atmospheric circulation patterns. *J. Geophys. Res.*, *98*(D9), 16653-16667.

Charles, S.P., Bates, B.C. and Hughes, J.P. (1999). A spatio-temporal model for downscaling precipitation occurrence and amounts. *J. Geophys. Res.,* 104(D24), 31657-31669.

Chatfield, C., and A. J. Collins, 1980. *Introduction to Multivariate Analysis.* Chapman and Hall, London, 246 pp.

Clark, C.O., Cole, J.E. and Webster, P.J. (2000). Indian Ocean SST and Indian summer precipitation: Predictive relationships and their decadal variability, *J. Climate, 13,* 2503-2519.

Cleveland, W.S. (1993). *Visualizing Data*. AT&T Bell Laboratories, New Jersey, 360 pp.

Crane, R.G. and Hewitson, B.C. (1998). Doubled CO_2 precipitation changes for the Susquehanna basin: down-scaling from the GENESIS general circulation model. *Int J Climatol., 18*, 65-76.

Enke, W. and Spekat, A. (1997). Downscaling climate model outputs into local and regional weather elements by classification and regression. *Clim. Res., 8*, 195-207.

Gates, W.L., Henderson-Sellers, A., Boer, G.J., Folland, C.K., Kitoh, A., McAvaney, B.J., Semazzi, F., Smith, N., Weaver, A.J. and Zeng, Q.-C. (1996). Climate models - evaluation. In: *Climate Change 1995: The Science of Climate Change*. Contribution of Working Group I to the Second Assessment Report of the Intergovernmental Panel on Climate Change, J.T. Houghton, L.G. Meira Filho, B.A. Callander, N. Harris, A. Kattenberg, and K. Maskell (ed.), Cambridge Univ. Press, Cambridge, 229-284.

Hines, K.M. and D.H. Bromwich (1999). Artificial surface pressure trends in the NCEP/NCAR Reanalysis over the Southern Ocean. Proc. of the Second WCRP International Conference on Reanalyses, Wokefield Park, UK, 23-27 August 1999. WCRP-109; WMO/TD-985, pp. 50-53.

Hughes, J.P., Guttorp, P. and Charles, S.P. (1999). A non-homogeneous hidden Markov model for precipitation occurrence. *Appl. Statist., 48* (1), 15-30.

Huth, R. (1997). Potential of continental-scale circulation for the determination of local daily surface variables. *Theor. Appl. Climatol., 56*, 165-186.

IOCI, (1999). *Towards Understanding Climate Variability in South Western Australia – Research Reports of the First Phase of the Indian Ocean Climate Initiative.* Indian Ocean Climate Initiative (IOCI), Perth, 237 p.

Jobson, J.D., 1992. A*pplied Multivariate Analysis.* Springer-Verlag, New York, 731 pp.

Kalnay, E. and Co-authors (1996). The NCEP/NCAR 40-year reanalysis project. *Bull. Amer. Meteor. Soc., 77*, 437-471.

Kshirsagar, A.M., 1972. *Multivariate Analysis.* Marcel Dekker, New York, 534 pp.

Manly, B.F.J., 1991. *Randomization and Monte Carlo Methods in Biology*. Chapman and Hall, London, 281 pp.

Marshall, G.J. and S.A. Harangozo (1999). A preliminary validation and analysis of NCEP/NCAR Reanalysis monthly MSLP data over the South Pacific/Southern Ocean region. Proc. of the Second WCRP International Conference on Reanalyses, Wokefield Park, UK, 23-27 August 1999. WCRP-109; WMO/TD-985, pp. 77-80.

McGregor, J.L., Gordon, H.B., Watterson, I.G., Dix, M.R. and Rotstayn, L.D. (1993). The CSIRO 9-level atmospheric general circulation model. *CSIRO Div. Atmos. Res. Tech. Paper No. 26*, 89 pp.

Qiu, P. and B. Yandell, 1998. A local polynomial jump-detection algorithm in nonparametric regression. *Technometrics*, **40**, 141-152.

Smith, I.N., McIntosh, P., Ansell, T.J., Reason, C.J.C. and McInnes, K. (2000). South-west Western Australian winter rainfall and its association with Indian Ocean climate variability. *Int. J. Climatol., 20,* 1913-1930.

Sturman, A. and Tapper, N. (1996). *The Weather and Climate of Australia and New Zealand*. Oxford University Press, Melbourne, 476 pp.

Tapp, R. and Cramb, J. (2000). *Some Aspects of Variability and Recent Trends in Rainfall in South-West Western Australia.* Bureau of Meteorology, Tech. Rept 72, May 2000, 28 p.

Venables, W.N. and Ripley, B.D. (1994). *Modern Applied Statistics with S-Plus.* Springer-Verlag, New York, 462 p.

Wilby, R.L., Hassan, H. and Hanaki, K. (1998). Statistical downscaling of hydrometeorological variables using general circulation model output. *J. Hydrol., 205*, 1-19.

APPENDIX A - GLOSSARY

General circulation   The global-scale wind system that largely determines the broad climate patterns on Earth.

Dew point temperature   Temperature to which air needs to be cooled for condensation to occur at a given atmospheric pressure and mixing ratio.

Downscaling   Quantification of the relation of local- and regional-scale climate variables to larger scale atmospheric patterns.   These patterns may be observed or simulated by dynamical climate models.

Dry spell   A sequence of consecutive days during which daily precipitation remains below 0.3 mm.

Front   The transition zone or interface between two air masses of contrasting wind, temperature and density.

Geopotential height   The work that must be done against gravity to raise a mass of 1 kg from sea-level to the level of interest in the atmosphere.

Markov process   A stochastic process in which the 'future' is determined by the 'present' and is independent of the 'past'.

Mean Sea Level Pressure   Total atmospheric pressure at the average height of the sea for all tidal stages over a 19-year period.

Mixing ratio   Ratio of the mass of water vapour to the mass of dry air in a given volume of air.

Precipitation   Any and all forms of water that falls from clouds and reaches the earth's surface.

Quantile   The value of a variable below which a certain proportion of the variable values will fall.

Wet spell   A sequence of consecutive days during which daily precipitation equals or exceeds 0.3 mm.

APPENDIX B - LIST OF ACRONYMS

BIC   Bayesian information criterion.

CAR   CSIRO Atmospheric Research

CCA   Canonical correlation analysis

CLW   CSIRO Land and Water.

EOF   Empirical orthogonal function

GCM   General circulation model.

GMT   Greenwich Mean Time: the 24-hour time scale used throughout the scientific and military communities. Other names for this time measurement are Universal Time Coordinate (UTC) and Zulu (Z).

CSIRO9   Spectral 9-level general circulation model developed by CSIRO Atmospheric Research.

IOCI   Indian Ocean Climate Initiative.

MSLP   Mean sea level pressure.

NCAR   National Center for Atmospheric Research.

NCEP   National Centers for Climate Prediction.

NHMM   Nonhomogeneous hidden Markov model

SLP   Sea level pressure

SST   Sea surface temperature.

SWA   Southwest Western Australia.